ASME Journal of Energy Resources Technology
Online journal at:
https://asmedigitalcollection.asme.org/energyresources

Conceptual Design of Experimental Test Rig for Research on Thermo-Flow Processes During Direct Contact Condensation in the Two-Phase Spray-Ejector Condenser

Paweł Madejski[1]
AGH University of Krakow,
Faculty of Mechanical Engineering and Robotics,
Department of Power Systems and Environmental Protection Facilities,
al. Adama Mickiewicza 30,
30-059 Kraków, Poland
e-mail: Pawel.madejski@agh.edu.pl

Michał Karch
AGH University of Krakow,
Faculty of Mechanical Engineering and Robotics,
Department of Power Systems and Environmental Protection Facilities,
al. Adama Mickiewicza 30,
30-059 Kraków, Poland
e-mail: karch@agh.edu.pl

Piotr Michalak
AGH University of Krakow,
Faculty of Mechanical Engineering and Robotics,
Department of Power Systems and Environmental Protection Facilities,
al. Adama Mickiewicza 30,
30-059 Kraków, Poland
e-mail: pmichal@agh.edu.pl

Krzysztof Banasiak
SINTEF Energy,
Trondheim 7034, Norway
e-mail: krzysztof.banasiak@sintef.no

The paper presents the conceptual design of a prototype experimental facility for mixing jet-type flow condensers investigations when the steam in exhaust gases is condensed on the water jet in the presence of CO_2. The proposed experimental test rig was designed to give abilities to investigate the effectiveness of jet condensers experimentally as part of the CO_2 capture phase and especially to investigate Spray-Ejector Condensers (SEC) developed as the combination of ejector and condenser devices. The paper presents the design and key features of the prototype installation components. The basic design was developed based on the simulation results, and for this purpose, model of installation, including characteristics of individual components, was built. The developed model helps to evaluate the main performances of the conceptual test rig and supports the test-rig design process. The main components and the features of the steam generation unit, CO_2 supply and mixing with steam, process water preparation, and H_2O and CO_2 separation subsystem are discussed. The measuring system was designed to test the efficiency of compression and condensation processes of the SEC fed by the CO_2/H_2O gas mixture. The performances of the two-phase jet condensers can be analyzed by experimental investigation and calculation of heat transferred to the cooling water during direct contact condensation with the presence of CO_2. The paper presents the results of heat flowrates and their uncertainties for the selected period of the experimental test, confirming the application of the novel developed test rig.
[DOI: 10.1115/1.4064194]

Keywords: alternative energy sources, energy conversion/systems, energy systems analysis, heat energy generation/storage/transfer

Introduction

Direct contact condensation (DCC) is widely used in various industries, and direct contact condensers are devices in which direct contact condensation is utilized. DCC has been widely used for over a century in multiple industrial applications such as petroleum and chemical engineering, desalination installations, and power plants [1]. In direct contact condensers, the cooling liquid is directly mixed with the gas or steam, leading to its condensation. This has a direct impact on the advantages of this solution compared to a surface condenser of the same capacity, such as smaller size [2], simpler construction, better corrosion resistance [3], lower cost [4], easier maintenance, and simpler operation [5]. Sideman and Moalem-Maron [6] reported that the advantages of direct contact condensation compared to conventional processes using metal transfer surfaces are due to the relative simplicity of design, fewer problems with corrosion and scaling, lower maintenance costs, higher specified transfer surfaces, and higher transfer rates. The authors report that DCC studies are usually associated with one-component, two-phase (vapor–water) systems, pure or containing trace amounts of non-condensable substances. DCC is inherently limited by the equilibrium between the latent heat of condensation and the sensible heat that the liquid can absorb until it is saturated. Spray-type direct contact condensers (ejector condensers) are commonly used in various applications, such as refrigeration cycles [7–10], desalination installations [11–13], and combined heat and power (CHP) systems [14,15]. They are also found in geothermal power plants [16,17] to reduce energy/exergy losses [18] and removal of non-condensable gases [19,20]. The latter application has gained increasing interest recently for possible use in

[1]Corresponding author.

Contributed by the Advanced Energy Systems Division of ASME for publication in the Journal of Energy Resources Technology. Manuscript received May 1, 2023; final manuscript received September 25, 2023; published online January 9, 2024. Assoc. Editor: Pawel Gladysz.

conventional thermal power plants due to the political constraints related to CO_2 emissions forcing the development of various CO_2 capture and storage (CCS) techniques [21,22], utilizing pre-combustion, post-combustion, or oxyfuel combustion approaches [23,24].

Chen et al. [25] simulated a 1000-MWe supercritical thermal power plant in the Aspen Plus software with a chemical looping air separation technology to produce oxygen used in the oxy-combustion process. The CO_2-rich gas stream, at high temperature, was supplied to the primary port of the ejector from the flue gas channel of the boiler. The flue gas at a lower temperature was bled and pressured at the second port. The flow ratio at these two inlets was adjusted to meet the chemical looping air separation (CLAS) process requirements. The power generation efficiency of the proposed plant was reduced by 1.37% in comparison to 3.97% for the supercritical power plant. Zhai et al. [26] proposed an integration of a solar energy system with a coal-fired power plant with a monoethanolamine (MEA)-based CCS. Simulations performed in EBSILON Professional and Aspen Plus programs. Two variants were considered. In the first one, the solar thermal system was used to heat the high-pressure feed water. In the second case, that system was used to heat the stripper's reboiler. Compared with the base case, without the solar system, the thermo-economic cost of electricity increased by 12.71% and decreased by 9.77% for the first and second solutions, respectively. Ding et al. [27] used the Matlab/Simulink platform to simulate the solid oxide fuel cell/gas turbine hybrid system with biogas as fuel and with an additional recirculation process by combustor exhaust gas. The ejector was used here to recirculate the exhaust gas with biogas fuel before entering the reformer. This way, a lower temperature gradient was achieved in the solid oxide fuel cell, and water for reforming reactions was supplied. Presented computations revealed that that process raised the electrical efficiency of the whole system from 58.2% to 62.8% Aspen Plus, Aspen Hysys, and Ebsilon codes were used to analyze the model of a negative CO_2 emission gas power plant using gasified sewage sludge as main fuel and based on oxy-combustion combined with a CCS system [28–30] and a spray-ejector condenser used to condense the water vapor from the exhaust gases. Simulated rated power and gross efficiency were in good agreement in all tools.

Simulation studies, however important at the design stage [31], should be verified in experiments to prove or disprove the validity of the assumptions and methods adopted. Various experimental studies on ejector condensers have been presented recently [32]. Zong et al. [33] and Yang et al. [34] experimentally investigated the impact of steam–water parameters on flow patterns (water mass flux in range, $6–18 \times 10^{-3}$ kg/m^{2}s; steam mass flux, 200–600 kg/m^{2}s; water pressure, 0.1–0.5 MPa), average heat transfer coefficient, and on pressure and temperature distributions in a rectangular mix chamber of the ejector condenser. Kwidzinski [35] analyzed heat and mass transfer in mixing chambers of four ejectors built to investigate passive safety systems for pressurized water reactors in laboratory conditions (steam pressure from 60 to 430 kPa, steam mass flowrate from 75 to 130 kg/h, water flowrate from between 1500 and 6500 kg/h, and water temperature of 14–40 °C). The empirical relationship for a condensate mass fraction at the mixing chamber outlet was proposed. Shah et al. [36–38] assessed experimentally the impact of the mixing section length on the transport process in the ejector condenser (steam pressure from 140 to 220 kPa, steam inlet temperature from 382 to 396 K, water inlet pressure 96 kPa, and water inlet temperature 290 K). The authors noticed an increasing water mass flowrate with increasing inlet steam pressure. Also, higher suction pressure and flowrate were obtained for a shorter length of the mixing section. Reddick et al. [39] presented results of an experimental test of a steam ejector's performance for a steam and carbon dioxide (as non-condensable gas) mixture (primary inlet pressure 350, 450, and 550 kPa, secondary in let pressure 50, 70, and 90 kPa). For pure steam, they noticed that a higher value of the primary pressure, secondary pressure, or nozzle diameter resulted in an increased critical pressure value and lower critical entrainment ratio. But entrainment of CO_2 resulted in the increased critical entrainment ratio while the critical pressure was unchanged. The experimental study of heat exchange with direct contact of water vapor with the water stream was the subject of the work [40]. Xu et al. investigated the condensation process of a stable steam jet in the water flow in a vertical pipe using a high-speed camera and a mobile thermocouple probe (maximum steam flowrate 0.03 kg/s, steam inlet pressure between 0.2 and 0.7 MPa, and steam inlet temperature from 110 to 170 °C). Condensation characteristics were investigated, including streak shape, flux length, temperature distribution, mean heat transfer coefficient, and mean Nusselt number. Zhang et al. [41] present the effect of non-condensing gas contained in a condensing gas on the characteristics of a gas-concentrated water ejector, where the gas is steam, water, and air, respectively, and liquid and non-condensing gas is the gas. The performance of the ejector expressed in the ejected water flowrate was found to increase firstly with a small amount of non-condensable gas and decrease when the non-condensable gas reaches a certain amount. In addition, the distributions of multiple local flow parameters, including pressure, condensation rate and gas volume fraction, velocity and temperature inside the ejector, were shown for different non-condensable concentration, by which the mechanism for the change of ejector performance under varying non-condensable concentration was demonstrated. Ghazi [42] investigated experimentally the direct contact heat transfer process of air injection through an orifice and bubbling through a constant temperature pool of water, which showed an air temperature increase of about 100–200%. Dehghani et al. [43] present the design of humidification–dehumidification desalination with direct contact dehumidifier system. The presented system was investigated experimentally under various operating conditions to find the influence of seawater and freshwater temperature and mass flowrates on system performances by utilizing non-dimensional parameters.

The detailed description of the concept, operating conditions, acquisition and monitoring system, together with the main assumptions for the implementation of the Spray-Ejector Condenser installation, was presented by Madejski et al. [44,45]. These studies investigated the selected crucial issues and possibilities for carrying out experimental research about DCC in the two-phase ejector condenser system. The testing activities were focused on the laboratory scale of the designed installation (steam and CO_2 mass flowrate around 10 g/s), taking into account opportunities to investigate the condensation process during flow through the two-phase ejector. Several studies on test rigs with direct contact condensers have been published recently. The Thermochemical Power Group (TPG) at the Polytechnic School of the University of Genoa built the first one. The authors studied a method of water introduction in a gas turbine circuit known as the humid air turbine (HAT) cycle. The humidification was provided by a column-pressurized saturator. The rig's design, mathematical model, and experimental results were described [46,47]. The maximum values of the following variables were set: operating pressure of the vessel of 5 bar, gas inlet temperature of 300 °C, liquid water inlet temperature of 135 °C, gas mass flowrate of 10 g/s, and liquid water mass flowrate of 10 g/s. An application of the direct contact condenser to enhance energy recovery from low-grade heat sources was studied in Refs. [48–50]. The condenser was made as a 70-cm-high Perspex column with a 4-cm internal diameter. Pentane vapor (the dispersed phase) with different initial temperatures was directly contacted with water (the continuous phase). During the tests, temperatures have not exceeded 50 °C. A rotameter was used for measuring the continuous phase (water) mass flowrate pumped from a 160-L storage tank. Kwidzinski [36,51] presented results of laboratory experiments with the low-pressure steam–water injector. The device was originally built to study passive safety systems for pressurized water reactors (PWR). Shah et al. [37] investigated a steam jet pump using the test rig with a steam boiler with a maximum flowrate of 52 kg/h at a maximum operating pressure of 8 bar. The authors studied the impact of geometrical parameters on the

operation of the device. These experimental studies, however important from the practical point of view, as providing necessary base for the test-rig design, were not devoted to CO_2 as the working gas. Such works also have been presented recently with the application of spray-ejector condensers in the recovery of flue gas waste heat and CO_2 in microalgae cultivation with power production [52], cryogenic removal of CO_2 from natural gas [53], noncondensable gases gas removal system [4], or cooling of the working fluid [54] in the geothermal power plant. The use of direct contact condensers with CO_2 in thermal power plants has recently been presented only in a few works. Amann et al. [55] simulated the energy and environmental performances of the natural gas combined cycle (NGCC) power plant with an O_2/CO_2 cycle and with a CO_2 recovery process based on a cryogenic separation of carbon dioxide from inert gases. An air separation unit generates the oxygen required. A spray condenser is used to condense the gaseous stream in the high-pressure part to supply heat to the low-pressure part.

The presented project contains a concept for developing a prototype research installation of a Spray-Ejector Condenser, which have to be applicable as a vapor steam condenser contained in a gas mixture (with inert gas CO_2) and generate a pressure lift of the water-gas mixture at the Spray-Ejector Condenser outlet. The need to develop a test rig to experimentally investigate the operation effectiveness of the designed Spray-Ejector Condenser in a thermal power plant for CO_2 separation emerged. In papers by Madejski et al. [56–58], the main assumptions for the simulations, during the conceptual design process and selection of measurement equipment for a test rig developed within the project scope, were presented. Based on the proposed assumptions, a test rig was built and then preliminary research was conducted. This study aims to cover this gap. For given reasons, the necessary simulations were performed at first. Using output values of process parameters, their variability ranges were defined as the base for the conceptual design of the test rig. The uncertainty analysis was performed with the preliminary experimental results for the selected time of spray-ejector condenser operation.

General Scheme of Prototype Experimental Test-Rig Installation

The presented test-rig facility is a prototype test rig for experimental research of two-phase jet-type flow condensers with a high share of inert gas and is equipped with the required systems:

- Superheated steam generation system with controllable temperature, pressure, and mass flux of steam.
- CO_2 supply system allows for control of temperature, pressure, and mass flux, together with the CO_2-steam mixing system.
- Water supply system to the water jet with adjusting of water temperature, pressure, and mass flux.
- Water/steam/CO_2 outlet mixture system of the tank for mixture separation into gas and liquid parts along with gas and a liquid outlet.
- System for special mounting and connection of the jet condenser under test to the test plant.
- A control and measurement system to record the necessary measurement signals and to control selected parameters of the plant operation.

Figure 1 presents the diagram of the developed test rig, including all systems. The prototype design test stand has assumptions that enable the implementation of the test on jet condensers, especially the possibility of feeding the ejector condenser with a gaseous mixture (water vapor/CO_2 mixture), feeding the condenser with cold water, the output of the mixture of water/steam/CO_2, and separation of the gaseous part from the liquid (water) part. Selected main parameters will perform condenser operation tests.

Spray-Ejector Condenser Operation Principles. The layout of the spray-ejector condensers is shown in Fig. 2. When a high-pressure motive fluid enters the nozzle and mixing chamber, this decreases pressure and increases the fluid's velocity. Next, the fluid enters the diffuser, resulting in an increasing pressure and decreasing fluid velocity due to the pressure difference vacuum created between the nozzle and diffuser. This negative pressure causes a mixture of water vapor and CO_2 suction. The mixture then enters the condenser, where the steam is condensed.

The spray-ejector condenser system consists of the following:

- A connection section for the cooling water (with adjustment of length and inlet diameter), together with pressure and temperature sensors to enable the connection of the ejector condenser.
- A connection section for a water vapor and CO_2 mixture, together with temperature and pressure sensors and a valve enabling mixture pressure regulation at the inlet to the ejector, together with temperature and pressure sensors.
- A steam/CO_2 mixture inlet section together with a bypass for directing the mixture to the separator.
- Water/steam/CO_2 connection for the water/steam/CO_2 mixture outlet (with possible length adjustment), together with pressure and temperature sensors.

The main goal of the test facility is to conduct experimental investigations of the spray-ejector condensers. The mathematical

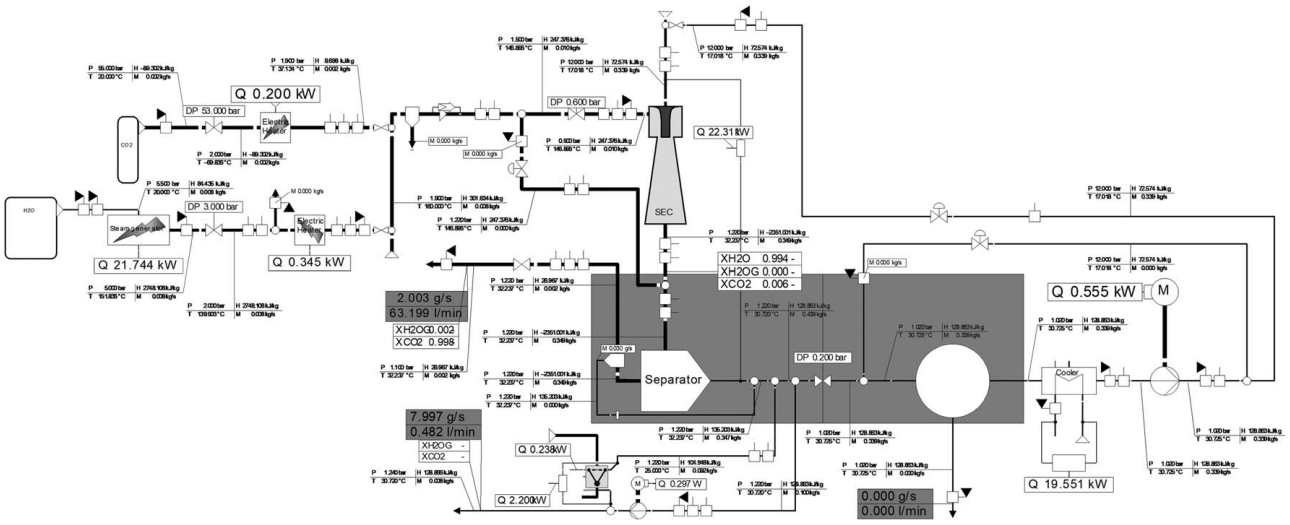

Fig. 1 Scheme and results of the basic parameters calculations for the designed prototype research installation

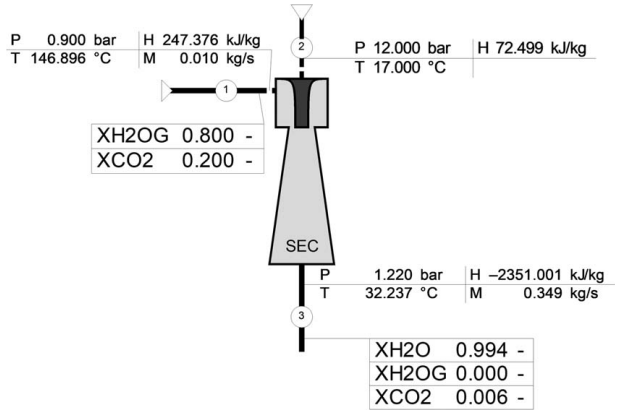

Fig. 2 Schematic of the connection system with the main thermodynamic parameters at the inlets and outlet (1—suction fluid inlet, 2—motive fluid inlet, 3—outlet)

description of this component is needed to identify the measured physical quantities. Figure 2 presents the spray-ejector condenser scheme. The considered ejector condenser consists of two inlets (motive liquid and suction gas section) and one outlet. In such a case, according to the mass (Eq. (1)) and energy balance (Eq. (2)), heat given by a mixture of water vapor and CO_2 is equal to the heat absorbed by cooling water:

$$\dot{m}_{1,H_2O} + \dot{m}_{1,CO_2} + \dot{m}_2 = \dot{m}_3 \tag{1}$$

$$\dot{Q}_{cw} = \dot{Q}_{eg} = \dot{Q}_{vap,cool} + \dot{Q}_{vap,cond} + \dot{Q}_{water,cool} + \dot{Q}_{CO_2,cool} \tag{2}$$

where $\dot{m}_{1,H_2O}$ is the mass flowrate of inlet steam, kg/s; $\dot{m}_{1,CO_2}$ is the mass flowrate of inlet inert gas CO_2, kg/s; $\dot{m}_2$ is the mass flowrate of cooling inlet water, kg/s; $\dot{m}_3$ is the mass flowrate of outlet mixture of water, steam, and CO_2, kg/s; $\dot{Q}_{cw}$ is the heat flowrate absorbed by the cooling water, W; $\dot{Q}_{eg}$ is the heat flowrate transferred from the exhaust gas, W; $\dot{Q}_{vap,cool}$ is the heat flowrate of water vapor cooling, W; $\dot{Q}_{vap,cond}$ is the heat flowrate of water vapor condensation, W; $\dot{Q}_{water,cool}$ is the heat flowrate of condensate cooling, W; $\dot{Q}_{CO_2,cool}$ is the heat flowrate of CO_2 cooling, W.

The $\dot{Q}_{cw}$ is heat transferred to the motive water from the cooling of the steam, cooling of CO_2, condensation of the steam, and cooling of the condensed steam (water).

The relation for heat of water vapor cooling $\dot{Q}_{vap,cool}$ can be expressed as follows:

$$\dot{Q}_{vap,cool} = \dot{m}_{1,H_2O} \cdot (h_{1,H_2O} - h_{sat,vap}) \tag{3}$$

Heat of condensation $\dot{Q}_{vap,cond}$:

$$\dot{Q}_{vap,cond} = \dot{m}_{1,H_2O} \cdot r \tag{4}$$

Heat of water condensate cooling $\dot{Q}_{water,cool}$:

$$\dot{Q}_{water,cool} = \dot{m}_{1,H_2O} \cdot (h_{sat,liq} - h_{3,H_2O}) \tag{5}$$

where:

$$h_{sat,liq} = h_{sat,vap} - r \tag{6}$$

Heat of CO_2 cooling $\dot{Q}_{CO_2,cool}$ is calculated using the formula:

$$\dot{Q}_{CO_2,cool} = \dot{m}_{1,CO_2} \cdot (h_{1,CO_2} - h_{3,CO_2}) \tag{7}$$

Heat absorbed by cooling water $\dot{Q}_{CW}$ can be expressed as ($\Delta T = t_3 - t_2$):

$$\dot{Q}_{CW} = \dot{m}_2 \cdot c_w \cdot \Delta T \tag{8}$$

Water vapor and liquid enthalpy values are determined using IF-97 steam tables [59], and the values of carbon dioxide enthalpy from National Institute of Standards and Technology (NIST) tables [60]. Mass flowrate and temperature should be measured for proper energy balance calculation. The indirect methods can determine heat flowrates given in Eqs. (3)–(8).

Water and CO_2 Separation Principles. In order to effectively separate the mixture at the outlet of the ejector (CO_2 + water), Fig. 3 shows the concept of making the separator. The lower part of the lance should be immersed in water to be cooled in a closed circuit. The outlet mixture of the stream (water/steam/CO_2) is introduced under increased pressure into the water tank, allowing the condensation process to be completed by contacting the steam with the cooling water. Water from reservoir 5 will go to overflow 6, where phase separation takes place: liquid phase goes to reservoir and outlet 9; gas phase through louver condenser 7 to outlet 10.

The system for removing the water/steam/CO_2 mixture, which includes the separator, is shown in Fig. 4. This system consists of:

Inlet of the vapor/water/CO_2 mixture from the test object.

- A mechanical separator for separation of the gaseous and liquid parts.
- A tank with an immersed separator, and with the water cooling system.
- Gas outlet section in the tank with, and valve enabling gas pressure control.
- Liquid outlet section, complete with valve.
- Pressure and temperature measuring sensors at the outlet of the condenser.
- Measuring sensors for pressure, temperature, and mass flow of gases (CO_2) at the separator outlet.
- Water temperature measuring sensors inside the tank with a separator (on the water from the cooler).
- Water outlet section to the water tank feeding the nozzles.

Basic Calculations of the Designed Test Rig

In order to design and select appropriate components for the prototype, research installation, calculations, and simulations of the operation of the entire system were performed. The calculation results indicated the required range of operating parameters for individual systems and components.

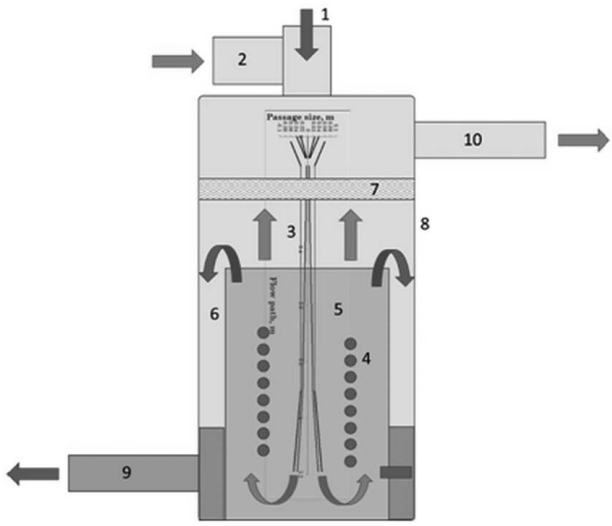

Fig. 3 The concept of implementation of an integrated condenser with phase separator and water cooler. 1—cooling water inlet, 2—gas mixture, 3—jet condenser, 4—cooling coil, 5—cooling water tank, 6—cooling water overflow, 7—mechanical condenser, 8—external water separator tank, 9—cooling water outlet, and 10—CO_2 gas outlet.

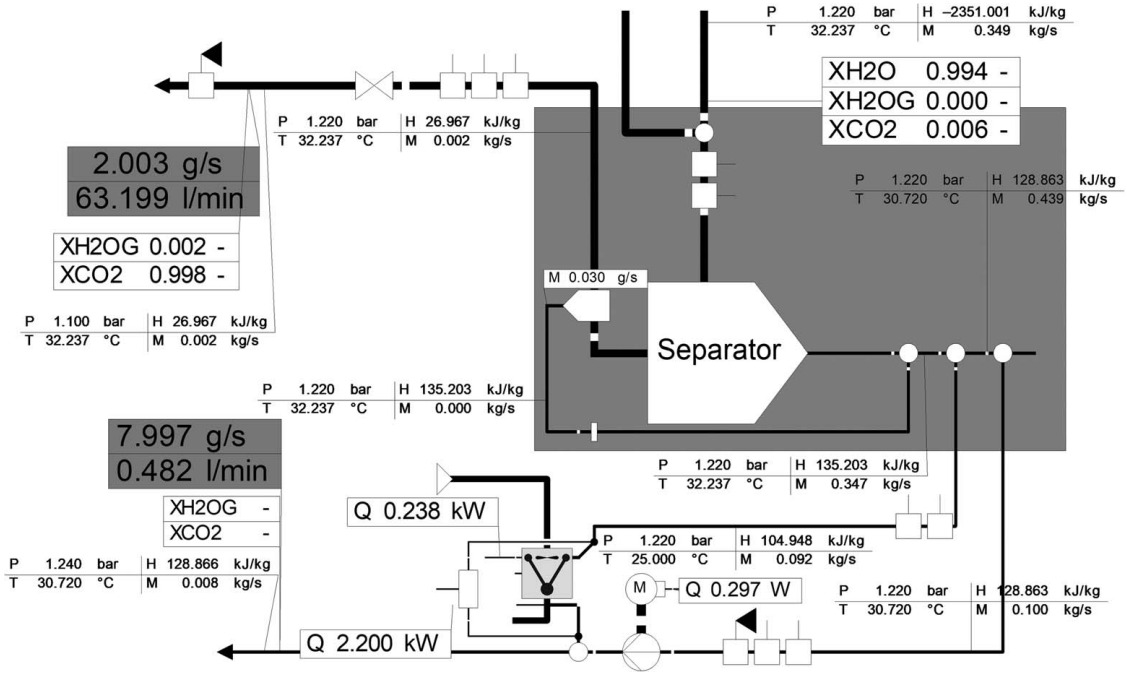

Fig. 4 Diagram of system (water/vapour/CO_2 mixture outlet to the tank for separation and mixture into gas and liquid part with gas and liquid outlet)

Table 1 Nominal operating parameters of the tested condenser for which the prototype research installation is designed

	Temperature (°C)	Pressure (bar)	Flow (kg/s)
Water inlet	17	12	Resulting
Gas inlet	150	0.2; 0.9	0.010
Outlet	Resulting	1.10; 1.15	Resulting

Table 2 The range of operating parameters that the designed research installation should enable for the purpose of carrying out experimental tests on an ejector condenser

	Temperature (°C)	Pressure (bar)	Flow (kg/s)
Water inlet	5–35	2–16	Resulting
Gas inlet	110–170	0.2–2.0	0.008–0.015
Outlet	Resulting	1–3	Resulting

Input Data for Designed Test Rig. At the stage of designing the stand, the following assumptions were made regarding the nominal operating parameters of the tested Spray-Ejector Condenser (Table 1). The main operating conditions resulted from the first condenser design stage, which should be examined and tested on the designed stand. For this purpose, the system must be equipped with components that allow adjusting the operating parameters in the range presented in Table 2.

Simulation Model of Proposed Test-Rig Installation. The ranges of the installation operating parameters have been selected considering the possibility of carrying out tests on condensers in a wide range of operations, not only at the nominal point. The diagram (Fig. 1) shows the example of calculations results of thermal and flow parameters at all points based on the simulation of the station's operation. The calculations were carried out for two selected variants of the condenser operation (gas pressure at the inlet 0.2 bar and 0.9 bar). Table 3 presents desired results for the two analyzed variants (Variant 1 and Variant 2).

Measuring Techniques and Sensors

Boundary conditions were defined with details to select measurement methods and devices properly. In the considered system, they should be understood as a variability range of basic thermodynamic variables, i.e., temperatures, pressures, and mass flows. Based on the performed simulations results, minimum and maximum

Table 3 Values of the basic parameters of the designed installation for the selected two variants of ejectors

	Variant 1	Variant 2
Water inlet pressure of the steam/CO_2 mixture at the inlet to the ejector	0.9 bar	0.2 bar
Water vapor stream at the inlet to the water jet	8 g/s	8 g/s
CO_2 Mass flow at the inlet to the ejector	2 g/s	2 g/s
Motive water mass flow at the inlet to the ejector	340 g/s	4399 g/s
Water, steam, and CO_2 mixture mass flow at ejector outlet	350 g/s	4409 g/s
Averaged mixture temperature at the ejector outlet	32.2 °C	18.4 °C
Electrical power of steam generator	21.74 kW	21.74 kW
Electrical power of CO_2 heater	0.2 kW	0.2 kW
Electrical power of steam superheater	0.345 kW	0.345 kW
Cooling unit power (separator tank + feed water tank)	21.75 kW	27.81 kW
Electrical power for water pump motor	0.55 kW	7.18 kW

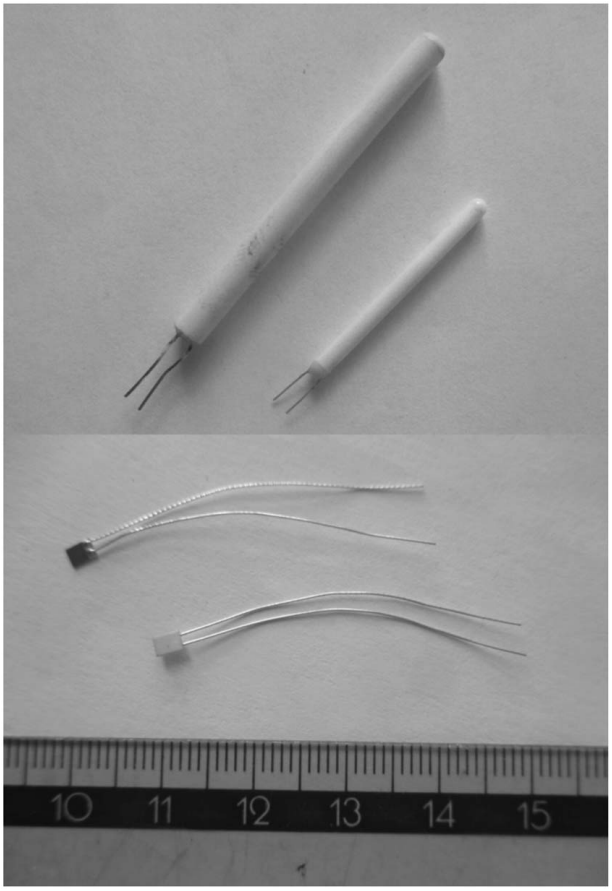

Fig. 5 Wire-wound (up) and thin-film (down) platinum RTDs

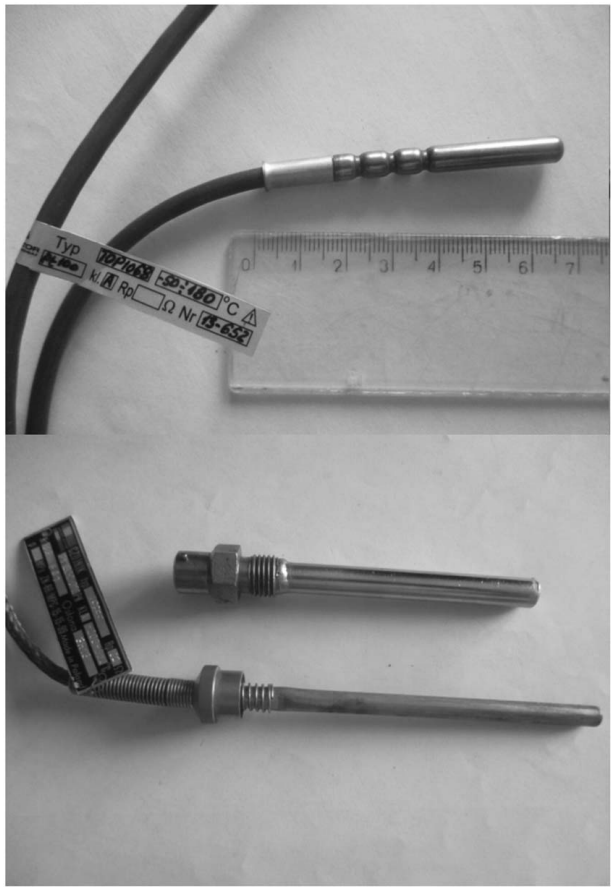

Fig. 6 Typical RTDs in sheaths

expected values of these parameters were assumed (Tables 1 and 2) to be taken into account in further consideration.

Temperature Measurement. The electrical sensors are part of the test-rig design. Hence, there was a choice between resistance temperature detectors (RTD) and thermocouples (TC). Both of them have pros and cons in certain conditions. Their basic features are discussed in the following sections taking into account the physical conditions of the considered test bed, especially that steam and water are electrically conductive process fluids. Two construction variants exist of RTDs [61–65], namely wire-wound and thin-film sensors (Fig. 5). Their length can be from about 2–3 millimeters to several centimeters. The sensor's length and the resistive wire's winding determine the measurement's character from "spot" to spatial.

To protect resistive winding against an impact of the external environment (corrosion, mechanical stress, etc.), the sensor is placed into an external sheath (Fig. 6), usually made of brass, steel, or ceramic material.

Using external sheath significantly impacts the thermal time constant of sensors, which is crucial when considering systems with rapidly varying temperatures. To illustrate this issue in Fig. 7, there is presented time response of various sensors with external sheaths which were immersed in water and ice mixture at a temperature of 0 °C and then placed into still air at a temperature of 20 °C. The fastest sensor (TOP1068) is shown in Fig. 6 (right). The second sensor (TOPE3) is shown in Fig. 6 on the right with (TOPE3-3H13) and without the additional sheath mounted in piping to allow fast replacement in case of failures. Hence, its thermal time constant is the lowest among the presented cases.

In thermocouples, the sensitive part of the sensor is the TC junction. Hence, the temperature measurement in this sensor is, in essence, of local type. However, sheaths are also used to protect the junction from the external environment. To reduce the thermal

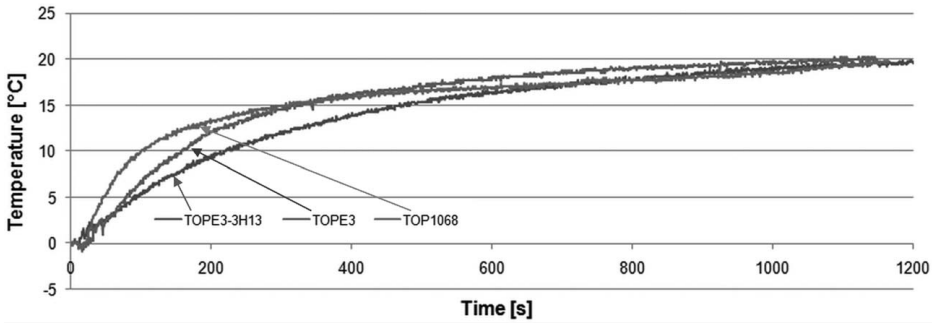

Fig. 7 Time response of various RTDs

time constant of the sensor, two different construction variants are used (Fig. 8), namely with grounded and ungrounded junctions. However, the first solution cannot be used when several sensors are mounted in electrically conducting materials like steel. Then, electrical loops are created, and a low-voltage signal from the thermocouple can be disturbed.

Appropriate thermal conditions should be created between the sensor and the measured substance to properly measure the surrounding liquid or gas temperature. The greater surface of the sensor results in higher mass and thermal time constant but improves heat transfer with the environment. When comparing these two kinds of sensors, their basic features should be taken into account [61]. The advantages of RTDs are their accuracy and stability. Because of their geometry, they are useful in the measurement of surface temperature. These sensors are more expensive, more fragile, larger, and have longer thermal response times. Also, a self-heating error occurs because of Joule's effect due to the flow of the electric current. For example, in Ref. [66], for the sensor in a sheath of 11 mm diameter, there are given values of T0.9 in well-mixed water for RTD, TC (isolated), and TC (grounded) of 120 s, 90 s, and 15 s, respectively. Thermocouples are relatively inexpensive, small, reasonably stable, and fast. Thermoelectric force is also independent of wire length and diameter. They are useful in the measurement of local temperature (point). But they are sensitive to electrical noise, bare thermocouples cannot be used in conductive fluids, and the dependence of the thermoelectric force on the temperature is nonlinear. In the considered test bed, well-developed flows are supposed to occur in CO_2, water, and steam piping. Hence, RTDs can preferably be used in these points. But when more local-directed measurements are needed, for example, to assess temperature distribution in the pipeline cross-section, then TCs are preferable. These tips are in line with the conclusions presented in the introduction.

Pressure Measurement. The pressure sensor selection for the test stand is based on the expected pressure values in measurement points and the maximum temperature of the working fluid. Piezoelectric transducers are commonly used among various electric pressure transducers due to their accuracy, stability, linearity, and favorable price. To reduce temperature errors, the sensitive components should be protected against the action of the high-temperature fluid. Typical working temperatures of piezoelectric transducers vary between 80 °C and 125 °C. However, in the designed test bed, the temperature of process fluids may reach 160–170 °C. Hence, additional protection should be used. Usually, two solutions are used. A non-insulated siphon tube directly in front of the pressure gauge, in which condensate or chilled water accumulates, protects the elastic component against high fluid temperature. Its length depends on the pressure sensor's working fluid temperature and maximum working temperature. It can be applied for process temperatures up to several hundred Celsius degrees. For temperatures of 200–300 °C, cooling components with special fins are used. Among various solutions, the S-20 pressure transmitter was recommended for general industrial applications manufactured by WIKA (Włocławek, Poland). An additional cooling component with five fins (Fig. 9) can be used to process medium temperatures up to 200 °C. In points where process temperature is below 125 °C, it can be used without any additional protecting components.

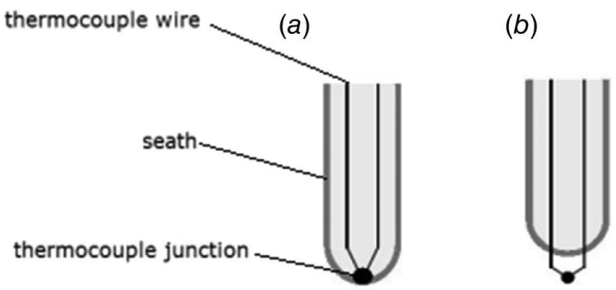

Fig. 8 (*a*) Grounded and (*b*) ungrounded thermocouples

Mass Flowrate Measurement. Mass flowrate measurement is technically difficult and complex issue. However, there exist a number of methods used in this category of measurement. Based on the literature review, a short summary of the most popular and commercially available measurement techniques can be successfully applied. The differential pressure flowmeters (orifice plate, Venturi tube, and nozzle) are simple and reliable when manufactured and installed following relevant standards. Their main disadvantage is pressure drop and their sensitivity to installation conditions. The turbine flow meters perform best when measuring clean, conditioned, steady flows of gases and liquids with low kinematic viscosities. Typical accuracy is of 0.25%. Electromagnetic flow meters can be used only for conductive liquids. Hence, they are not suitable for gas flow. Typical accuracy can be 0.5–1%. Impurities of liquids and the contact resistances of the electrodes can worsen accuracy to the value of 5%. Ultrasonic flowmeters can be applied in nearly any kind of flowing liquid providing no obstruction to flow. Two types are in use: Doppler and transit time. They are sensitive to entrained gas bubbles reflecting the ultrasonic beam. Also, solid particles scatter the ultrasonic wave. The advantages of a vortex flow meter are independence of measured volumetric flow on the fluid density, simple construction, lack of moving parts, and good operation with liquids and gases. These sensors create pressure drops comparable to orifice plates or turbine meters. Typically it has 1% accuracy. Coriolis flow meters directly measure the mass flow of fluids of different densities and viscosities. They can also measure the mass flow of two-phase mixtures, liquid–liquid (such as emulsions) and liquid–solid. The operation of thermal flow meters is based on the principle that the rate of heat absorbed by a flowing fluid is directly proportional to the mass flowrate. These meters are theoretically applicable to measuring liquid flows. But, in practice, they are used mostly in gas flow measurements, but particulates and condensates should be avoided. Typical accuracy is of 2%. For further consideration, the following most important points and measurement devices were selected:

- CO_2 at the inlet to the ejector: thermal flow meter (mass flowrate),
- steam at the outlet of the steam generator: vortex flow meter (mass flowrate),
- steam and CO_2 mixture at the inlet to the ejector: vortex flow meter (mass flowrate).
- motive water mass flow at the inlet to the ejector: electromagnetic flow meter (volume flowrate).

CO_2 Content Measurement. Measurement of CO_2 content is technically a demanding issue due to this gas's physical and chemical properties. Several methods are currently in use in technical applications, and several CO_2 sensors possibly would be applicable in the designed test rig [68]. There are as follows:

- potentiometric sensors—Severinghaus;
- potentiometric sensors—Solid electrolyte sensors;
- non-dispersive infrared (NDIR) CO_2 sensors.

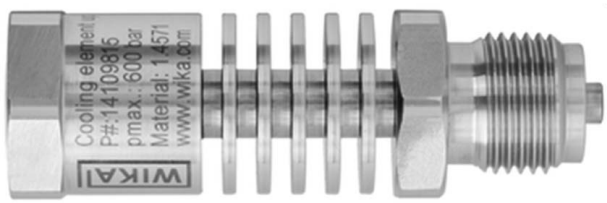

Fig. 9 Cooling component with five fins [67]

The disadvantage of potentiometric sensors is the need to calibrate them before starting measurements. The calibration of electrochemical CO_2 sensors is difficult if measurements under field conditions and in solutions of unknown and changing composition must be carried out. Their typical response time T0.9 is between 30 s and 120 s, measuring temperature up to 50 °C. Solid electrolyte sensors are, in principle, similar to the above mentioned. For physical reasons, operational temperature is typically within the 200–750 °C range. In the case of semiconductors—from −10 to 100 °C, additional power is required to heat the sensor when working in low temperatures. Output electrical signal depends on gas concentration, response time is typically below 1 s, and they do not require calibration, but can be used only in gas applications. NDIR sensors use the concentration-dependent absorption of electromagnetic radiation in the IR range. Their typical response time is between 5 and 30 s, and the typical operating temperature is 0–50 °C. Modern solutions have in-build converters that have self-calibration functions. Measurement of CO_2 dissolved in water is technically troublesome, because it requires longer time and stable conditions. The concentration of gaseous CO_2 can be estimated using commercially available NDIR sensors.

Data Acquisition System. A device with simultaneous sampling of measured inputs is recommended for data acquisition system. That device should have a number of analogue inputs equal to the number of measurement sensors. Typical output signals from sensors are recommended in voltage (0–10 V) or current (4–20 mA) standards. The latter is safer from a practical perspective because zero current means failure occurred in the circuit. In case of no voltage, this state can be interpreted as zero value of the measured quantity or as a fault in the system. Flow meters are usually equipped with current (4–20 mA) and pulse/frequency outputs proportional to the value of the measured quantity. Considerations presented in the introductory section indicate that the possible solution should allow data recording with a time stamp from about 0.1–1 s to about 10 min.

Accuracy and Uncertainty of Spray-Ejector Condenser Tests Results. Using the propagation model of uncertainty [69,70], the standard combined uncertainty u_c of y is calculated using the following formula:

$$u_c(y) = \sqrt{\left(\frac{\partial y}{\partial x_1}u(x_1)\right)^2 + \left(\frac{\partial y}{\partial x_2}u(x_2)\right)^2 + \ldots + \left(\frac{\partial y}{\partial x_n}u(x_n)\right)^2} \quad (9)$$

Then, the expanded uncertainty is calculated from the equation:

$$U = ku_c(y) \quad (10)$$

Usually, when $k = 2$ is applied, it means a 95% level of confidence [70]. Applying Eqs. (2)–(4), (6), and (7) into (9), the following relationships for the measurement uncertainties of the relevant heat flowrates, starting from the uncertainty of heat absorbed by cooling water, are as follows:

$$u_c(\dot{Q}_{cw}) = \sqrt{\left(\frac{\partial \dot{Q}_{cw}}{\partial \dot{m}_{cw}}u(\dot{m}_{cw})\right)^2 + \left(\frac{\partial \dot{Q}_{cw}}{\partial c_w}u(c_w)\right)^2 + \left(\frac{\partial \dot{Q}_{cw}}{\partial \Delta T}u(\Delta T)\right)^2} \quad (11)$$

Uncertainty of the cooling water mass flowrate $u(\dot{m}_{cw})$ can be assessed based on the data provided by the manufacturer of the flow meter. Uncertainty of the specific heat of water $u(c_w)$ can be assumed at ±0.03% [71]. For water vapor cooling:

$$u_c(\dot{Q}_{vap,cool}) = \sqrt{\left(\frac{\partial \dot{Q}_{vap,cool}}{\partial \dot{m}_{1,H_2O}}u(\dot{m}_{1,H_2O})\right)^2 + \left(\frac{\partial \dot{Q}_{vap,cool}}{\partial h_{1,H_2O}}u(h_{1,H_2O})\right)^2 + \left(\frac{\partial \dot{Q}_{vap,cool}}{\partial h_{sat,vap}}u(h_{sat,vap})\right)^2} \quad (12)$$

Steam enthalpy uncertainty, defined at selected temperature and pressure, according to IF-97 and NIST tables within the region of interest, is ±0.2% [72]. The uncertainty of CO_2-specific enthalpy is equal to 0.95% [73].

Uncertainty of heat of condensation:

$$u_c(\dot{Q}_{vap,cond}) = \sqrt{\left(\frac{\partial \dot{Q}_{vap,cond}}{\partial \dot{m}_{1,H_2O}}u(\dot{m}_{1,H_2O})\right)^2 + \left(\frac{\partial \dot{Q}_{vap,cond}}{\partial r}u(r)\right)^2} \quad (13)$$

Uncertainty of heat of water condensate cooling $\dot{Q}_{water,cool}$:

$$u_c(\dot{Q}_{water,cool}) = = \sqrt{\left(\frac{\partial \dot{Q}_{water,cool}}{\partial \dot{m}_{1,H_2O}}u(\dot{m}_{1,H_2O})\right)^2 + \left(\frac{\partial \dot{Q}_{water,cool}}{\partial h_{sat,liq}}u(h_{sat,liq})\right)^2 + \left(\frac{\partial \dot{Q}_{water,cool}}{\partial h_{3,H_2O}}u(h_{3,H_2O})\right)^2} \quad (14)$$

And finally uncertainty of heat of CO_2 cooling:

$$u_c(\dot{Q}_{CO_2,cool}) = = \sqrt{\left(\frac{\partial \dot{Q}_{CO_2,cool}}{\partial \dot{m}_{1,CO_2}}u(\dot{m}_{1,CO_2})\right)^2 + \left(\frac{\partial \dot{Q}_{CO_2,cool}}{\partial h_{1,CO_2}}u(h_{1,CO_2})\right)^2 + \left(\frac{\partial \dot{Q}_{CO_2,cool}}{\partial h_{3,CO_2}}u(h_{3,CO_2})\right)^2} \quad (15)$$

Using presented relationships, measurement uncertainties can be estimated at given known operating conditions.

Results and Discussion of Experimental Two-Phase Ejector Performances Evaluation

The diagram of the designed test installation is shown in Fig. 10. It consists of several parts that perform separate functions. These are the sections: steam production, CO_2 supply, steam and CO_2 mixture preparation, process water supply, condensate and vacuum production.

It is made from the following main components: steam generator, steam superheater, water pump, and water chiller. The electric boiler with the additional superheater provides steam to the ejector. Water pump supplied by the controlled inverter provides motive water for the ejector within the pressure range of inlet water from 0 to 16 bar. The chiller is used to cool the outlet

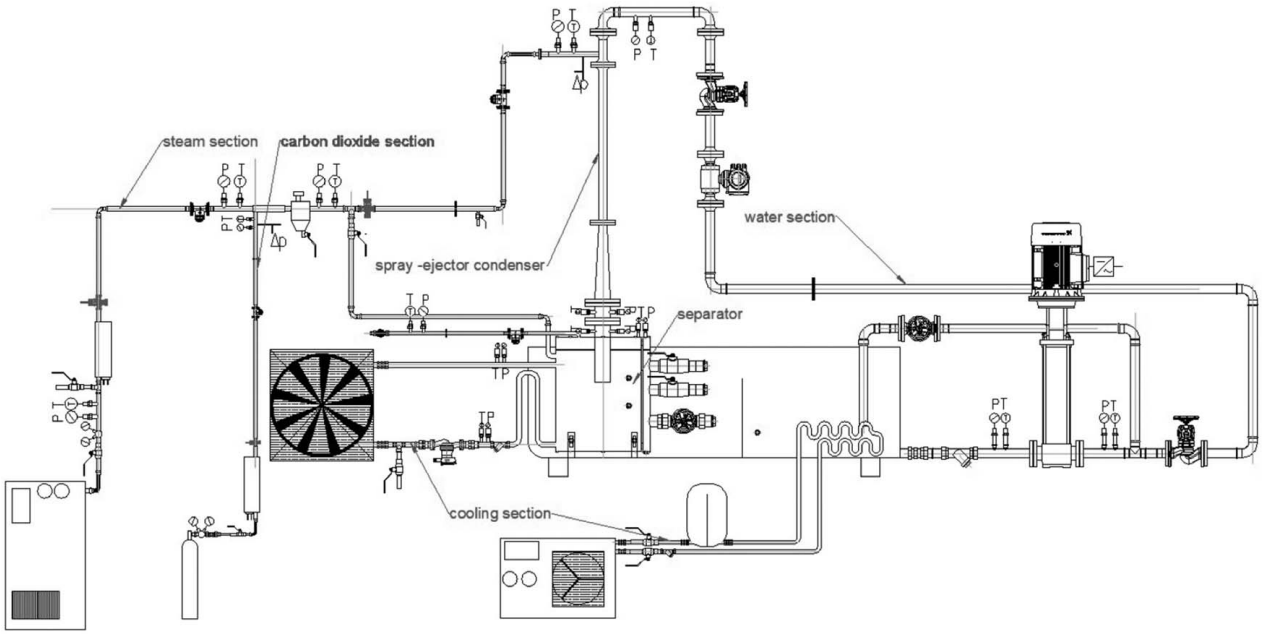

Fig. 10 Diagram of the designed research installation

water from the ejector in the water tank, which is then reused and supplied by the water pump. CO_2 is supplied from the CO_2 tank by the CO_2 heater to the mixer, which is mixed with superheated steam and then supplied to the ejector. The test rig was also equipped with appropriate pressure, temperature, and flow measuring devices. Their layout is given in Fig. 11. The FT, PT, and TT symbols mean mass flow, pressure, and temperature transmitters. The basic data on their measuring ranges and accuracies are provided in Table 4. Accuracy class A of Pt100 sensors in accordance with EN ISO 60751. Flowmeter for mixture and FW flowmeters measure volume flow while flowmeter for CO_2 (FC) and FS measure mass flow.

To evaluate the accuracy of the outputs obtained with the use of the experimental test facility, the measurement results were

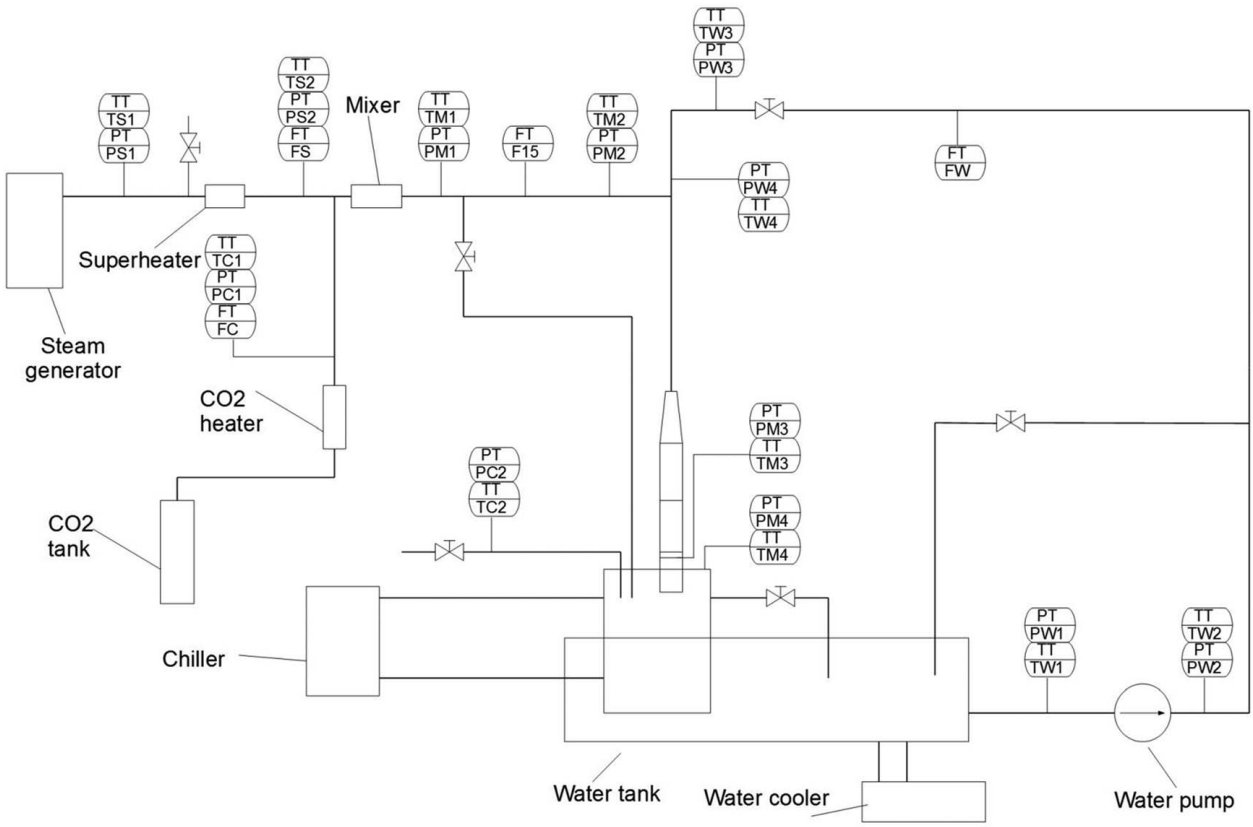

Fig. 11 Location of measurement sensors of temperature (TT), pressure (PT), and mass flowrate (FT)

Table 4 Measuring ranges and accuracy of used sensors

Symbol	Range/class	Error	Type/Manufacturer
PW1, PW2, PW3, PW4	0–16 bar	$\leq \pm 1\%$ of full scale	A-10, WIKA
TW1, TW2, TW3, TW4, TM3, TM4	0–150 °C, Pt100, class A	0.1 K or 0.08% of full scale	APTOPGB-11, Limatherm
FW	0.1–6.0 kg/s (20 °C, 1.5 bar)	2.3%–0.5% of measured value (volume flow)	Promag H300, Endress + Hauser
TM2, TM1, TS2, TS1, TC1, TC2	0–300 °C, class A	0.2% of full scale	TOPE-L0384, Limatherm
PM1, PM2, PM3, PM4, PS1, PS2, PC1, PC2	0–2.5 bar	$\leq \pm 0.5\%$ of full scale	S-20, WIKA
FM	5–13 g/s (200 °C, 1.5 bar)	1% of measured value (volume flow)	Prowirl F200, Endress + Hauser
FS	5–10 g/s (200 °C, 1.5 bar)	1.1% of measured value (mass flow)	Prowirl F200, Endress + Hauser
FC	0.1–2.0 g/s (100 °C, 1.0 bar)	3–1% of measured value (mass flow)	t-mass F300, Endress + Hauser

Table 5 Results of measured values and the calculated value of outlet mass flowrate

Point	t, °C	p, bar	$\dot{m}$, g/s
1	97.07	−0.0428	7.879 (vapor) 1.789 (CO_2)
2	27.82	14.76	336.0
3	41.64	−0.0028	345.669

Table 6 Calculated values of heat flowrate and uncertainty of $\dot{Q}_{cw}$, $\dot{Q}_{vap,cool}$, $\dot{Q}_{vap,cond}$, $\dot{Q}_{water,cool}$, and $\dot{Q}_{CO_2,cool}$ based on the registered measured values with the use of experimental test-rig facility

Parameter	Unit	Value
$u_c(\dot{Q}_{cw})$	kW	0.31
$u_c(\dot{Q}_{vap,cool})$	kW	0.06
$u_c(\dot{Q}_{vap,cond})$	kW	0.2
$u_c(\dot{Q}_{water,cool})$	kW	0.023
$u_c(\dot{Q}_{CO_2,cool})$	kW	0.013
$\dot{Q}_{cw}$	kW	19.40 ± 0.62
$\dot{Q}_{vap,cool}$	kW	0.0 ± 0.12
$\dot{Q}_{vap,cond}$	kW	17.80 ± 0.40
$\dot{Q}_{water,cool}$	kW	1.886 ± 0.046
$\dot{Q}_{CO_2,cool}$	kW	0.089 ± 0.026

taken at a sampling time of 10 s during the 2 min of quasi-stable thermal and flow conditions and averaged (Table 5). For measured values at ejector boundary points, the uncertainties and heat flowrates were calculated (Table 6) using Eqs. (3)–(5), (7), (8), and (11)–(15).

Results of simulation for two different basic designs of spray-ejector condensers (Variant 1 and Variant 2) allowed determine pressure, temperature, and mass flow ranges in the most important points of the whole circuit. Test-rig operation was designed for the boundary conditions of inlet water (17 °C; 12 bar; 340/4399 g/s) and steam/CO_2 mixture (150 °C; 0.2/0.9 bar; 10 g/s) to the spray-ejector condenser.

The highest heat flow value transferred to the cooling water during direct contact condensation is heat flowrate of steam condensation $\dot{Q}_{vap,cond} = 17.80 \pm 0.40$. Cooling condensed steam to the outlet mixture temperature t_3 also impacts the total heat transferred to the cooling water $\dot{Q}_{water,cool} = 1.886 \pm 0.046$, while the heat of CO_2 cooling is insignificant. For the presented case, steam at the inlet to the spray-ejector condenser was not superheated, and the total heat of steam cooling is equal to 0. The developed concept of a test rig allows for conducting experimental research on thermo-flow processes during direct contact condensation in the two-phase spray-ejector condensers.

Conclusions

The paper presents the conceptual design of a novel experimental test-rig facility for mixing jet-type flow condensers and spray-ejector condenser investigations, together with the idea of water–CO_2 separation. Presented test-rig design focus on the possibility of experimentally investigating direct contact condensation in two-phase ejectors, when the motive water can reach a large range of mass flowrate and sucked gas can be a steam or steam and inert gas mixture. When the gas is a mixture of steam and CO_2 (inert gas), the impact of different gas share at the inlet on the two-phase ejector performances can be investigated. The presented idea is ready for implementation, and experimental research outputs can be used to develop the most effective jet-type flow condensers with the application for oxy-combustion novel gas power plants. The simulation results of the test-rig operation with the use of the developed 0D balance model supported the design process. The simulation model was built, and variability ranges of input parameters were tested to define final operating conditions and select proper devices such as steam generator, CO_2 heater, tanks, pipes, sensors, and instrumentation adaption strategy.

Nominal conditions of the main components needed for the building of the test-rig experimental installation were selected. Based on them, the most appropriate measurement techniques dedicated to temperature, pressure, mass flow, and CO_2 concentration were discussed and recommended in terms of the design assumptions. Finally, the data acquisition system was proposed. The possibility of spray-ejector condenser performance analysis with the use of a designed test-rig is confirmed by the calculation of heat flowrates during direct contact condensation of the steam with the presence of CO_2. Heat transferred to the motive cooling water during the cooling of the steam, cooling of CO_2, condensation of the steam, and cooling of the condensed steam (water) was calculated thanks to the measured values for the selected 2 min period of quasi-stable thermal and flow operation.

The presented conceptual design is challenging when the constant operating conditions of gas are required. Hot steam is produced constantly and mixed with CO_2 with reduced pressure and low temperature (pressure reduction in the gas bottle from 200 bar to 1 around bar). Keeping appropriate gas properties in a long time of experimental investigation requires simultaneously heating steam producing, steam superheating, and CO_2 heating. This challenge is possible to avoid by implementing CO_2 heaters set or by using longer time data registration of each case. The original design of the Spray-Ejector Condenser required building a novel prototype installation for experimental investigations of two-phase ejectors when direct contact condensation occurs with the presence of inert gas.

The described idea of building a test rig for this kind of experimental research is a novel approach, and all operating conditions were developed to investigate the spray-ejector condenser—an individual and one of the critical components of the oxy-combustion gas power plant. The presented conceptual design was implemented, and experimental research on Spray-Ejector

Condensers has already been done for the various operating conditions.

Funding Data

- The research leading to these results has received funding from the Norway Grants 2014–2021 via the National Centre for Research and Development, Poland. Work has been prepared within the frame of the project: "Negative CO_2 emission gas power plant"—NOR/POLNORCCS/NEGATIVE-CO_2-PP/0009/2019-00 which is co-financed by the programme "Applied research" under the Norwegian Financial Mechanisms 2014–2021 POLNOR CCS 2019—Development of CO_2 capture solutions integrated into power and industry processes.

Conflict of Interest

There are no conflicts of interest.

Data Availability Statement

The datasets generated and supporting the findings of this article are obtainable from the corresponding author upon reasonable request.

Nomenclature

k = constant, $k = 2$
r = latent heat of H_2O, kJ/kg
U = expanded uncertainty
c_w = specific heat of water, kJ/kgK
$h_{sat,liq}$ = enthalpy of saturated liquid/H_2O at point 1, kJ/kg
$h_{sat,vap}$ = enthalpy of saturated vapor/H_2O at point 1, kJ/kg
h_{1,CO_2} = enthalpy of CO_2 at point 1, kJ/kg
h_{3,CO_2} = enthalpy of CO_2 at point 3, kJ/kg
h_{1,H_2O} = enthalpy of H_2O at point 1, kJ/kg
h_{3,H_2O} = enthalpy of H_2O at point 3, kJ/kg
t_3 = temperature of mixture at point 3, K
t_2 = temperature of water at point 1, K
$\dot{m}_{1,H_2O}$ = mass flowrate of H_2O at point 1, kg/s
$\dot{m}_{1,CO_2}$ = mass flowrate of CO_2 at point 1, kg/s
$\dot{m}_2$ = mass flowrate of cooling water at point 2, kg/s
$\dot{m}_3$ = mass flowrate of outlet mixture of water, steam, and CO_2, kg/s
$\dot{Q}_{cw}$ = heat flowrate absorbed by the cooling water, W
$\dot{Q}_{eg}$ = heat flowrate transferred from the exhaust gas, W
$\dot{Q}_{vap,cool}$ = heat flowrate transferred from the exhaust gas, W
$\dot{Q}_{vap,cond}$ = heat flowrate of water vapor condensation, W
$\dot{Q}_{water,cool}$ = heat flowrate of condensate cooling, W
$\dot{Q}_{CO_2,cool}$ = heat flowrate of CO_2 cooling, W
ΔT = temperature difference of cooling water, K
$u_c(y)$ = uncertainty of variable y

References

[1] Boehm, R. F., and Kreith, F., 1988, "Direct-Contact Heat Transfer Processes," *Direct-Contact Heat Transfer*, F. Kreith, and R. F. Boehm, eds., Springer, Berlin/Heidelberg, Germany.
[2] Chantasiriwan, S., 2015, "Effects of Cooling Water Flow Rate and Temperature on the Performance of a Multiple-Effect Evaporator," Chem. Eng. Commun., **202**(5), pp. 622–628.
[3] Zhao, X., Fu, L., Sun, T., Wang, J. Y., and Wang, X. Y., 2017, "The Recovery of Waste Heat of Flue Gas From Gas Boilers," Sci. Technol. Built Environ., **23**(3), pp. 490–499.
[4] Prananto, L. A., Juangsa, F. B., Iqbal, R. M., Aziz, M., and Soelaiman, T. A. F., 2018, "Dry Steam Cycle Application for Excess Steam Utilization: Kamojang Geothermal Power Plant Case Study," Renewable Energy, **117**(1), pp. 157–165.
[5] Sanopoulos, D., and Karabelas, A., 1997, "H2 Abatement in Geothermal Plants: Evaluation of Process Alternatives," Energy Sources, **19**(1), pp. 63–77.
[6] Sideman, S., and Moalem-Maron, D., 1982, "Direct Contact Condensation," Adv. Heat Transfer, **15**(1), pp. 227–281.
[7] Aidoun, Z., Ameur, K., Falsafioon, M., and Badache, M., 2019, "Current Advances in Ejector Modeling, Experimentation and Applications for Refrigeration and Heat Pumps. Part 1: Single-Phase Ejectors," Inventions, **4**(1), p. 15.
[8] Aidoun, Z., Ameur, K., Falsafioon, M., and Badache, M., 2019, "Current Advances in Ejector Modeling, Experimentation and Applications for Refrigeration and Heat Pumps. Part 2: Two-Phase Ejectors," Inventions, **4**(1), p. 16.
[9] Zhao, H., Zhang, K., Wang, L., and Han, J., 2016, "Thermodynamic Investigation of a Booster-Assisted Ejector Refrigeration System," Appl. Therm. Eng., **104**(1), pp. 274–281.
[10] Almohammadi, B. A., Alharthi, M. A., Siddiqui, M. A., and Kumar, R., 2021, "Investigation of a Combined Refrigeration and Air Conditioning System Based on Two-Phase Ejector Driven by Exhaust Gases of Natural Gas Fueled Homogeneous Charge Compression Ignition Engine," ASME J. Energy Resour. Technol., **143**(12), p. 120911.
[11] Dong, J., Wang, W., Han, Z., Ma, H., Deng, Y., Su, F., and Pan, X., 2018, "Experimental Investigation of the Steam Ejector in a Single-Effect Thermal Vapor Compression Desalination System Driven by a Low-Temperature Heat Source," Energies, **11**(9), p. 2282.
[12] Ali, E. S., Mohammed, R. H., Qasem, N. A. A., Zubair, S. M., and Askalany, A., 2021, "Solar-Powered Ejector-Based Adsorption Desalination System Integrated With a Humidification-Dehumidification System," Energy Convers. Manag., **238**(1), p. 114113.
[13] Ren, J., Zhao, H., Wang, M., Miao, C., Wu, Y., and Li, Q., 2022, "Design and Investigation of a Dynamic Auto-Adjusting Ejector for the MED-TVC Desalination System Driven by Solar Energy," Entropy, **24**(12), p. 1815.
[14] Borisov, I., Khalatov, A., and Paschenko, D., 2022, "The Biomass Fueled Micro-Scale CHP Unit With Stirling Engine and Two-Stage Vortex Combustion Chamber," Heat Mass Transfer, **58**(7), pp. 1091–1103.
[15] Li, X., Li, X., and Akhatov, J. S., 2020, "Feasibility and Performance Study of Solar Combined Heat and Power System With Absorption Heat Pump in Uzbekistan," Appl. Sol. Energy, **56**(6), pp. 498–507.
[16] Potapov, V. V., Podverbnyi, V. M., Gorbach, V. A., and Taskin, V. V., 2007, "Composition of Corrosion Products and Solid Deposits in the Flow Path of the Verkhnemutnovsk Geothermal Power Station," Therm. Eng., **54**(8), pp. 607–613.
[17] Tomarov, G. V., and Shipkov, A. A., 2017, "Modern Geothermal Power: GeoPP With Geothermal Steam Turbines," Therm. Eng., **64**(3), pp. 190–200.
[18] Mondal, S., Sahana, C., and De, S., 2022, "Optimum Operation of a Novel Ejector Assisted Flash Steam Cycle for Better Utilization of Geothermal Heat," Energy Convers Manage., **253**(1), p. 115164.
[19] Ozcan, N. Y., and Gokcen, G., 2009, "Thermodynamic Assessment of Gas Removal Systems for Single-Flash Geothermal Power Plants," Appl. Therm. Eng., **29**(14–15), pp. 3246–3253.
[20] Idzon, O. M., Ivanov, V. V., Ilyushin, V. V., and Nikol'skii, A. I., 2004, "Process Control System of the Mutnovskaya Geothermal Power Plant," Power Technol. and Eng., **38**(1), pp. 41–48.
[21] Notz, R. J., Tönnies, I., McCann, N., Scheffknecht, G., and Hasse, H., 2011, "CO_2 Capture for Fossil Fuel-Fired Power Plants," Chem. Eng. Technol., **34**(2), pp. 163–172.
[22] Madejski, P., Chmiel, K., Subramanian, N., and Kuś, T., 2022, "Methods and Techniques for CO_2 Capture: Review of Potential Solutions and Applications in Modern Energy Technologies," Energies, **15**(3), p. 887.
[23] Czakiert, T., Krzywanski, J., Zylka, A., and Nowak, W., 2022, "Chemical Looping Combustion: A Brief Overview," Energies, **15**(4), p. 1563.
[24] Hatta, N. S. M., Aroua, M. K., Hussin, F., and Gew, L. T., 2022, "A Systematic Review of Amino Acid-Based Adsorbents for CO_2 Capture," Energies, **15**(10), p. 3753.
[25] Chen, S., Hu, J., Sun, Z., and Xiang, W., 2018, "Application of Chemical Looping Air Separation for MILD Oxy-Combustion in the Supercritical Power Plant With CO_2 Capture," Energy Sci. Eng., **6**(5), pp. 490–505.
[26] Zhai, R., Liu, H., Wu, H., Yu, H., and Yang, Y., 2018, "Analysis of Integration of MEA-Based CO_2 Capture and Solar Energy System for Coal-Based Power Plants Based on Thermo-Economic Structural Theory," Energies, **11**(5), p. 1284.
[27] Ding, X., Lv, X., and Weng, Y., 2019, "Coupling Effect of Operating Parameters on Performance of a Biogas-Fueled Solid Oxide Fuel Cell/Gas Turbine Hybrid System," Appl. Energy, **254**(1), p. 113675.
[28] Ziółkowski, P., Badur, J., Pawlak-Kruczek, H., Niedzwiecki, L., Kowal, M., and Krochmalny, K., 2020, "A Novel Concept of Negative CO_2 Emission Power Plant for Utilization of Sewage Sludge," Proceedings of the 6th International Conference on Contemporary Problems of Thermal Engineering CPOTE 2020, Gliwice, Poland, Sept. 21–24, pp. 531–542.
[29] Ziółkowski, P., Madejski, P., Amiri, M., Kuś, T., Stasiak, K., Subramanian, N., Pawlak-Kruczek, H., Badur, J., Niedźwiecki, Ł, and Mikielewicz, D., 2021, "Thermodynamic Analysis of Negative CO_2 Emission Power Plant Using Aspen Plus, Aspen Hysys, and Ebsilon Software," Energies, **14**(19), p. 6304.
[30] Ziółkowski, P., Stasiak, K., Amiri, M., and Mikielewicz, D., 2023, "Negative Carbon Dioxide Gas Power Plant Integrated With Gasification of Sewage Sludge," Energy, **262**(Part B), p. 125496.
[31] Tashtoush, B. M., Moh'd, A. A.-N., and Khasawneh, M. A., 2019, "A Comprehensive Review of Ejector Design, Performance, and Applications," Appl. Energy, **240**(1), pp. 138–172.
[32] Madejski, P., Kuś, T., Michalak, P., Karch, M., and Subramanian, N., 2022, "Direct Contact Condensers: A Comprehensive Review of Experimental and Numerical Investigations on Direct-Contact Condensation," Energies, **15**(24), p. 9312.

[33] Zong, X., Liu, J.-P., Yang, X.-P., and Yan, J.-J., 2015, "Experimental Study on the Direct Contact Condensation of Steam Jet in Subcooled Water Flow in a Rectangular Mix Chamber," Int. J. Heat Mass Transfer, **80**(1), pp. 448–457.
[34] Yang, X. P., Liu, J. P., Zong, X., Chong, D. T., and Yan, J. J., 2015, "Experimental Study on the Direct Contact Condensation of the Steam Jet in Sub-Cooled Water Flow in a Rectangular Channel: Flow Patterns and Flow Field," Int. J. Heat Fluid Flow, **56**(1), pp. 172–181.
[35] Kwidzinski, R., 2021, "Condensation Heat and Mass Transfer in Steam–Water Injectors," Int. J. Heat Mass Transfer, **164**(1), p. 120582.
[36] Shah, A., Chughtai, I. R., and Inayat, M. H., 2011, "Experimental and Numerical Analysis of Steam Jet Pump," Int. J. Multiphase Flow, **37**(10), pp. 1305–1314.
[37] Shah, A., Chughtai, I. R., and Inayat, M. H., 2013, "Experimental Study of the Characteristics of Steam Jet Pump and Effect of Mixing Section Length on Direct-Contact Condensation," Int. J. Heat Mass Transfer, **58**(1-2), pp. 62–69.
[38] Shah, A., Chughtai, I. R., and Inayat, M. H., 2014, "Experimental and Numerical Investigation of the Effect of Mixing Section Length on Direct-Contact Condensation in Steam Jet Pump," Int. J. Heat Mass Transfer, **72**(1), pp. 430–439.
[39] Reddick, C., Sorin, M., Sapoundjiev, H., and Aidoun, Z., 2018, "Effect of a Mixture of Carbon Dioxide and Steam on Ejector Performance: An Experimental Parametric Investigation," Exp. Therm. Fluid Sci., **92**(1), pp. 353–365.
[40] Xu, Q., Guo, L., Zou, S., Chen, J., and Zhang, X., 2013, "Experimental Study on Direct Contact Condensation of Stable Steam Jet in Water Flow in a Vertical Pipe," Int. J. Heat Mass Transfer, **66**(1), pp. 808–817.
[41] Zhang, Y., Qu, X., Zhang, G., Leng, X., and Tian, M., 2020, "Effect of Non-Condensable Gas on the Performance of Steam-Water Ejector in a Trigeneration System for Hydrogen Production: An Experimental and Numerical Study," Int. J. Hydrogen Energy, **45**(39), pp. 20266–20281.
[42] Ghazi, H. S., 1991, "Direct-Contact Heat Transfer for Air Bubbling Through Water," ASME J. Energy Resour. Technol., **113**(2), pp. 71–74.
[43] Dehghani, S., Mahmoudi, F., Date, A., and Akbarzadeh, A., 2019, " Experimental Performance Evaluation of Humidification–Dehumidification System With Direct-Contact Dehumidifier," ASME J. Energy Resour. Technol., **142**(1), p. 012005.
[44] Madejski, P., Kuś, T., Subramanian, N., Karch, M., and Michalak, P., 2021, "The Possibilities of Carrying Out Numerical and Experimental Tests of Jet Type Flow Condensers for Application in Energy Technologies," Proceedings of the Wdzydzeanum Workshop on Fluid-Solid Interaction, Books of Abstract, Gdańsk, Poland, Sept. 5–10, p. 38.
[45] Madejski, P., Karch, M., Michalak, P., Banasiak, K., Kuś, T., and Subramanian, N., 2021, "Measurement Techniques and Apparatus for Experimental Studies of Flow Processes in a System With a Jet Flow Type Condenser," Proceedings of the XIV Multiphase Workshop and Summer School, Koszałkowo–Wieżyca k/Gdańska, Poland, Sept. 2–4, p. 28.
[46] Pedemonte, A. A., Traverso, A., and Massardo, A. F., 2008, "Experimental Analysis of Pressurised Humidification Tower for Humid Air Gas Turbine Cycles. Part A: Experimental Campaign," Appl. Therm. Eng., **28**(14–15), pp. 1711–1725.
[47] Caratozzolo, F., Traverso, A., and Massardo, A. F., 2011, "Implementation and Experimental Validation of a Modeling Tool for Humid Air Turbine Saturators," Appl. Therm. Eng., **31**(16), pp. 3580–3587.
[48] Mahood, H. B., Sharif, A. O., Al-Aibi, S., Hawkins, D., and Thorpe, R., 2014, "Analytical Solution and Experimental Measurements for Temperature Distribution Prediction of Three-Phase Direct-Contact Condenser," Energy, **67**(1), pp. 538–547.
[49] Mahood, H. B., Sharif, A. O., and Thorpe, R. B., 2015, "Transient Volumetric Heat Transfer Coefficient Prediction of a Three-Phase Direct Contact Condenser," Heat Mass Transfer, **51**(2), pp. 165–170.
[50] Mahood, H. B., Campbell, A. N., Baqir, A. S., Sharif, A. O., and Thorpe, R. B., 2018, "Convective Heat Transfer Measurements in a Vapour-Liquid-Liquid Three-Phase Direct Contact Heat Exchanger," Heat Mass Transfer, **54**(6), pp. 1697–1705.
[51] Kwidzinski, R., 2019, "Experimental and Theoretical Investigations of two-Phase Flow in Low Pressure Steam–Water Injector," Int. J. Heat Mass Transfer, **144**(1), p. 118618.
[52] Malek, A., Alamoodi, N., Almansoori, A. S., and Daoutidis, P., 2017, "Optimal Dynamic Operation of Microalgae Cultivation Coupled With Recovery of Flue Gas CO_2 and Waste Heat," Comput. Chem. Eng., **105**(1), pp. 317–327.
[53] Babar, M., Bustam, M. A., Maulud, A. S., Ali, A., Mukhtar, A., and Ullah, S., 2020, "Enhanced Cryogenic Packed Bed With Optimal CO_2 Removal From Natural Gas; A Joint Computational and Experimental Approach," Cryogenics, **105**(1), p. 103010.
[54] Gokcen, G., Ozturk, H. K., and Hepbasli, A., 2004, "Overview of Kizildere Geothermal Power Plant in Turkey," Energy Convers. Manage., **45**(1), pp. 83–98.
[55] Amann, J.-M., Kanniche, M., and Bouallou, C., 2009, "Natural Gas Combined Cycle Power Plant Modified Into an O_2/CO_2 Cycle for CO_2 Capture," Energy Convers. Manage., **50**(3), pp. 510–521.
[56] Madejski, P. J., Karch, M., Michalak, P., and Banasiak, K., 2022, "Conceptual Design of Experimental Test Rig for Research on Thermo-Flow Processes During Direct Contact Condensation in the Two-Phase Spray-Ejector Condenser," Proceedings of the 7th International Conference on Contemporary Problems of Thermal Engineering CPOTE 2022, Poland, Sept. 20–23, Conference Proceedings, pp. 909–920. https://www.s-conferences.eu/ftp/cpote/CPOTE_proceedings_19_10.pdf
[57] Madejski, P., Banasiak, K., Ziółkowski, P., Mikielewicz, D., Mikielewicz, J., Kuś, T., Karch, M., et al., 2022, "Development of a Spray-Ejector Condenser for the Use in a Negative CO_2 Emission Gas Power Plant," Proceedings of the 7 th International Conference on Contemporary Problems of Thermal Engineering CPOTE 2022, Poland, Sept. 20–23, Conference Proceedings, pp. 909–920. https://www.s-conferences.eu/ftp/cpote/CPOTE_proceedings_19_10.pdf
[58] Madejski, P., Michalak, P., Karch, M., Kuś, T., and Banasiak, K., 2022, "Monitoring of Thermal and Flow Processes in the Two-Phase Spray-Ejector Condenser for Thermal Power Plant Applications," Energies, **15**(19), pp. 7151.
[59] Wagner, W., and Kretzschmar, H. J., 2002, *International Steam Tables. Properties of Water and Steam Based on the Industrial Formulation IAPWS-IF97: Tables, Algorithms, Diagrams*, Springer-Verlag, Berlin Heidelberg, Germany.
[60] National Institute of Standards and Technology, "Carbon Dioxide Tables," https://webbook.nist.gov/cgi/inchi/InChI%3D1S/CO2/c2-1-3, Accessed September 9, 2022
[61] Michalski, L., Eckersdorf, K., Kucharski, J., and McGhee, J., 2001, *Temperature Measurement*, 2nd ed., John Wiley & Sons Ltd., San Francisco, CA.
[62] Lee, T.-W., 2008, *Thermal and Flow Measurements*, CRC Press, Taylor & Francis Group, LLC, Boca Raton, FL.
[63] Webster, J. G., and Eren, H., 2014, *Measurement, Instrumentation, and Sensors Handbook*, CRC Press, Boca Raton, FL.
[64] Loughlin, C., 1993, "Temperature Sensing," *Sensors for Industrial Inspection*, Springer, Dordrecht.
[65] Lipták, B. G., and Venczel, K., 2007, *Measurement and Safety*, CRC Press, Boca Raton, FL.
[66] "Temperature Probes," Catalogue. http://kompart-pomiary.pl/czujniki/czujniki%20temperatury.pdf
[67] "Cooling Component for Pressure Measuring Instruments," For Threaded Attachment. Model 910.32. https://www.wika.com/en-en/910_32.WIKA, Accessed June 20, 2022
[68] Smith, C. L., 2009, *Basic Process Measurements*, John Wiley & Sons, Inc, Hoboken, NJ.
[69] Helm, I., Jalukse, L., and Leito, I., 2010, "Measurement Uncertainty Estimation in Amperometric Sensors: A Tutorial Review," Sensors, **10**(5), pp. 4430–4455.
[70] Adamkowski, A., Janicki, W., Lewandowski, M., and da Costa Bortoni, E., 2021, "Uncertainty Analysis of Liquid Flow Rate Measurement With the Pressure–Time Method," Measurement, **185**(1), p. 109866.
[71] Popiel, C. O., and Wojtkowiak, J., 1998, "Simple Formulas for Thermophysical Properties of Liquid Water for Heat Transfer Calculations (From 0 °C to 150 °C)," Heat Transfer Eng., **19**(3), pp. 87–101.
[72] Advisory Note No. 1. Uncertainties in Enthalpy for the IAPWS Formulation 1995 for the Thermodynamic Properties of Ordinary Water Substance for General and Scientific Use (IAPWS-95) and the IAPWS Industrial Formulation 1997 for the Thermodynamic Properties of Water and Steam (IAPWS-IF97). The International Association for the Properties of Water and Steam. Vejle, Denmark, August 2003. http://www.iapws.org/relguide/Advise1.pdf, Accessed February 20, 2023
[73] Wang, J., Jia, C.-S., Li, C.-J., Peng, X.-L., Zhang, L.-H., and Liu, J.-Y., 2019, "Thermodynamic Properties for Carbon Dioxide," ACS Omega, **4**(21), pp. 19193–19198.